AIAA SciTech
5-9 January 2015, Kissimmee, Florida
53rd AIAA Aerospace Sciences Meeting

# Helicopter Blade NACA 8H12 Performance Prediction with Laminar-Turbulent Transition Effects: Integral Boundary-Layer and CFD Results compared with Experimental Data

Guilherme Araujo Lima Da Silva[1]
*ATS4i Aero-Thermal Solutions for Industry, São Paulo, SP, Brazil*

Donizeti de Andrade[2]
*Instituto Tecnológico de Aeronáutica, São José dos Campos, São José dos Campos, SP, Brazil*

Caio Fuzaro Rafael[3]
*Federal University of ABC, Santo André, SP, Brazil*

Diogo Mendes Pio[4]
*ATS4i Aero-Thermal Solutions for Industry, São Paulo, SP, Brazil*



**The present paper shows integral boundary-layer solutions and finite-volume Reynolds-Averaged Navier Stokes (RANS) Computational Fluid Dynamics (CFD) results for flow around a NACA 8H12 airfoil profile. The objective of the present paper is to verify and compare a CFD tool with traditional integral code results and experimental data in two subsonic Reynolds numbers: $1.8\text{x}10^6$ and $2.6\text{x}10^6$, where open literature experimental data exist for NACA 8H12 airfoil. An incompressible boundary-layer code coupled with external potential flow solution can be adequate for subsonic Reynolds ranges with ideal airfoils but has limitations for applications in compressible-flow regime, notably out of the correlation corrections range, in presence of massive separation at high angles of attack, particularly when one is trying to solve actual airfoil shapes. A numerical code that solves integral equations of boundary layer - with transition onset and length predictions as well as the intermittency evolution - is implemented based on literature models. Both CFD and integral code results are compared with experimental data for pressure, drag, lift and moment coefficients. The results show that laminar-turbulent transition consideration is very important to represent actual airfoil aerodynamics performance.**

## Nomenclature

| | | |
|---|---|---|
| $a$ | = | constant for Walz method |
| $b$ | = | constant for Walz method |
| $C_f$ | = | skin friction coefficient |
| $C_p$ | = | pressure coefficient |
| $C_{D,viscous}$ | = | viscous forces coefficient |
| $c$ | = | chord of airfoil |
| $F(H)$ | = | function of shape factor |
| $F(\lambda)$ | = | function of pressure gradient |
| $G(H)$ | = | function of shape factor |
| $H$ | = | shape factor, displacement thickness and momentum thickness ratio |

[1] Associate, PhD, Aerospace Division, Rua Cotoxó, 611 cj. 63, AIAA Member
[2] Professor, PhD, Aeronautical Engineering Department
[3] Trainee at ATS4i, Undergraduate student, Aerospace Engineering Department
[4] Associate, CFD Division, Rua Cotoxó, 611 cj. 63

$H_1$ = shape factor in fuction of $G(H)$
$H(\lambda)$ = shape factor in function of pressure gradient
$I(\lambda)$ = function of pressure gradient
M = Mach number
$Re_L$ = reference L length Reynolds number
$Re_{\delta 2}$ = momentum thickness Reynolds number
$s$ = surface coordinates
$Tu, \tau$ = turbulence level
$U_\infty$ = freestream velocity – far field
$u$ = velocity
$u_e$ = boundary-layer edge velocity
$v_E$ = flow velocity
$x_f$ = position where $u_e$ is maximum
$x_s$ = x position of the separation point
$y$ = y position of the boundary layer profile
$Z$ = function in Walz method
$\alpha$ = angle of attack
$\alpha_1$ = momentum thickness ratio
$\Gamma$ = shape parameter of velocity profile
$\gamma$ = intermittency factor
$\delta$ = boundary layer thickness
$\delta_1$ = displacement thickness
$\delta_2$ = momentum thickness
$\eta$ = turbulent spot production rate
$\eta_{crit}$ = function of $\tau'$
$\lambda$ = pressute gradient parameter
$\nu$ = dynamic viscosity
$\sigma$ = turbulent spot propagation parameter
$\tau'$ = function of turbulence level

***Subscripts***

0 = initial
$air$ = air properties
$lam$ = laminar
$stag$ = stagnation
$sep$ = separation
$tr, t$ = transition
$turb$ = turbulent
$\Delta s$ = length of separation



## I. Introduction

The present paper shows integral boundary-layer solutions and finite-volume Reynolds-Averaged Navier Stokes (RANS) Computational Fluid Dynamics (CFD) results for flow around a NACA 8H12 airfoil profile. Typically an original or some modified versions of NACA 8H12 airfoil are used in main rotor blade of helicopters and other rotorcraft applications.

From a validated set of results and an engineering assessment, one can carefully use the CFD numerical tool to predict aerodynamic performance at higher Mach and higher angles of attack than the validated range. Therefore CFD tool can be used as an extrapolation tool to predict performance of modified NACA 8H12 airfoils, where no experimental data exist yet, especially during preliminary design before the tunnel test campaign. For example, only a compressible flow solver can be applied to studies of Mach divergence problems, a very important information in the early phases of helicopter design. An incompressible boundary-layer code coupled with external potential flow solution can be adequate for subsonic Reynolds ranges with ideal airfoils but has limitations for applications in compressible-flow regime, notably out of the correlation corrections range, in presence of massive separation at high angles of attack, particularly when one is trying to solve realistic airfoils.

The mentioned airfoil – which has experimental data available – has been simulated with CFD tool along with two boundary-layer codes: 1) a numerical code that solves integral equations of boundary-layer - with transition onset and

length predictions as well as the intermittency evolution - is implemented based on literature models; 2) additionally, as a double check, XFoil[1, 2] is used due its proven reliability in aerodynamics calculations within its validity range. Both boundary-layer codes, one providing integral and another differential solution, served as traditional engineering baseline but also as tools to understand the underlying physics phenomena.

On the other hand, a modern RANS solver, CFD++[3, 4], has been adopted as tool due its broader general applicability than boundary-layer codes coupled – iteratively or not - with external flow solution. Its simulations takes into account effects of compressibility, turbulence and solution of the 2D flow field near and far from airfoil surface. However, it is important to emphasize that a differential code - like CFD++ and Xfoil- represent more accurately the flow history - including the pressure gradient gradient variation - than an integral code, which uses only local flow properties.

Results from CFD, Xfoil and integral code are compared with integral experimental data like $C_P$,$C_L$, $C_D$ and $C_M$ coefficients. Other boundary-layer local flow parameters like $C_f$ and $H$ are compared only code-to-code in order to verify results but mainly to understand the laminar-turbulent transition process. All the codes have models to handle or at least estimate laminar-turbulent transition onset prediction caused not only by natural mechanisms but also by separation bubbles and bypass transition mechanisms.

## II. Objective

The objective of the present paper is to verify and compare a CFD tool with traditional integral code results and experimental data in two subsonic $Re_L$, $1.8 \cdot 10^6$ and $2.6 \cdot 10^6$, where open literature experimental data exist for NACA 8H12 airfoil[5].

## III. Models Description

### A. CFD ++

CFD++, a RANS flow solver with realizable K-ε[6] and the Langtry-Menter[7-8] (LM) turbulence models. The first is a realizable version – original of CFD++ software - of the traditional two-equation K-ε. In present paper, no transition model was used in association with K-ε, despite CFD++ offers the transition as an option for K-ε. Therefore, it is fully turbulent since front stagnation to trailing edge. In general, its use is recommended for very low, low and even transonic M in some cases. The present authors could have also selected other turbulence models like SST and Spalart-Almaras since CFD++ offers these also as turbulence models. However, the comparison of turbulence models for fully turbulent flow is out of scope of the present paper. The second turbulence model used herein is a four-equation (SST+$R_\theta$+γ) with transition onset prediction and intermittency development models. It is laminar since front stagnation point. Transition will occur if one of the two conditions occur: laminar separation bubble or transported $Re_\theta$ predicts transition. Some authors

[10] validated the CFD results with test data when using a turbulence model with transported γ equation implemented by them. As a benchmark for the new $\gamma$ equation implementation in CFD solver, they compared also the results with boundary-layer codes – integral and differential - for laminar, turbulent and transition region

[10], where the intermittency γ goes from zero to unity.

### B. XFoil

The code XFoil has been used not only to code-to-code verifications but also to compare with experimental data. Its limitations due to potential flow solutions when applied to thick airfoil shape, high angles of attack and transonic Mach numbers are not important in the present paper since the airfoil is NACA 8H12 and M is low, i.e., thin airfoil in a subsonic flow. For actual airfoil shape – high thickness and sharp finite trainling tab, high angles of attack and compressible flow conditions, like the ones found in actual helicopter rotor blade operation, XFoil will not be within its valid limits of execution.

### C. Proposed Boundary-Layer Mathematical Model

The present paper proposes a mathematical model to represent the boundary-layer around the NACA 8H12 airfoil in order to estimate its aerodynamic performance. The aim is to allow a comparison of a solution from integral equation system to the solution of a modern CFD model for a flow with laminar-turbulent transition at low Re and low M. When comparing the results, the authors aimed to verify CFD results with a traditional and validated method[11] and to understand the main advantages of use of CFD in a two-dimensional, low Re and low M flow case. After a successful verification, the CFD can be used as extrapolation tool in a pre-design phase to simulate a flow cases out of limits of a mathematical model based on integral equations. For sure, further CFD validation will require future comparisons

with tunnel and flight experimental data - three-dimensional, high Re and high M with laminar-turbulent transition – in order to provide accurate means to model flow around actual helicopter blades.

The proposed model has some differences from previous works of Silva[12-14] and it intends to extend the modeling approach to flow around airfoils with strong pressure gradient variations and to consider the occurrence of laminar-turbulent transition at start or along of a laminar separation bubble. In some cases presented herein, the laminar separation occurs in a position upstream the natural or by-pass transition onset. Due to distortion or inflection in velocity profile within separation region, the laminar flow may be unstable and so more susceptible to transition to turbulent flow. Those disturbances in velocity profile can be seen in *H* variation upstream or along separated region.

*Watz's Laminar Boundary Layer[15]*

$$\boldsymbol{\delta_{2,lam}} = \left(\boldsymbol{Z}\frac{\boldsymbol{\nu_{air}}}{\boldsymbol{u_e}}\right)^{\mathbf{0.5}} + \boldsymbol{\delta_0} \tag{1}$$

$$\boldsymbol{Z(s)} = \frac{\boldsymbol{a}}{\boldsymbol{u_e}^{\boldsymbol{b}}}\int_{\boldsymbol{s_{stag}}}^{\boldsymbol{s_{tr}}} \boldsymbol{u_e}^{\boldsymbol{b}}\ \boldsymbol{ds} \tag{2}$$

$$\boldsymbol{C_{f,lam}} = \frac{\mathbf{2}\,\boldsymbol{\nu_{air}}\,\boldsymbol{u_e}\,\boldsymbol{\alpha_1}}{\boldsymbol{\delta_{2,lam}}\,\boldsymbol{U_\infty}^{\mathbf{2}}} \tag{3}$$

$$\begin{aligned} \boldsymbol{a} &= \mathbf{0.441}\,;\boldsymbol{b} = \mathbf{4.165} \quad \boldsymbol{\Gamma} > \mathbf{0} \\ \boldsymbol{a} &= \mathbf{0.441}\,;\boldsymbol{b} = \mathbf{4.579} \quad \boldsymbol{\Gamma} < \mathbf{0} \end{aligned} \tag{4}$$

$$\boldsymbol{\Gamma} = \frac{\boldsymbol{Z}}{\boldsymbol{u_e}}\frac{\boldsymbol{du_e}}{\boldsymbol{ds}} \tag{5}$$

Where $\alpha_1$ is obtained with interpolation of Hartree profiles.

*Head's Model for Turbulent Boundary Layer[16-18]*

$$\frac{\boldsymbol{v_E}}{\boldsymbol{u_e}} \equiv \frac{\mathbf{1}}{\boldsymbol{u_e}}\frac{\boldsymbol{d}}{\boldsymbol{ds}}\int_{\mathbf{0}}^{\boldsymbol{\delta}} \boldsymbol{u}\,\boldsymbol{dy} = \frac{\mathbf{1}}{\boldsymbol{u_e}}\frac{\boldsymbol{d}}{\boldsymbol{ds}}\left[\boldsymbol{u_e}(\boldsymbol{\delta} - \boldsymbol{\delta_1})\right] = \boldsymbol{F(H)} \tag{6}$$

$$\boldsymbol{H_1} = \frac{\boldsymbol{\delta} - \boldsymbol{\delta_1}}{\boldsymbol{\delta_2}} \tag{7}$$

$$\frac{\boldsymbol{d}}{\boldsymbol{ds}}\left(\boldsymbol{u_e}\boldsymbol{\delta_2}\boldsymbol{H_1}\right) = \boldsymbol{u_e}\,\boldsymbol{F} \tag{8}$$

$$\boldsymbol{H_1} = \boldsymbol{G(H)} \tag{9}$$

$$\boldsymbol{F} = \mathbf{0.0306}\,(\boldsymbol{H_1} - \mathbf{3.0})^{\mathbf{-0.6169}} \tag{10}$$

$$\boldsymbol{G} = \begin{cases} \mathbf{0.8234}\,(\boldsymbol{H} - \mathbf{1.1})^{\mathbf{-1.287}} + \mathbf{3.3}\,, & \boldsymbol{H} \le \mathbf{1.6} \\ \mathbf{0.5501}\,(\boldsymbol{H} - \mathbf{0.6778})^{\mathbf{-3.064}} + \mathbf{3.3}\,, & \boldsymbol{H} \ge \mathbf{1.6} \end{cases} \tag{11}$$

$$\boldsymbol{C_{f,turb}} = \mathbf{0.246}\,\mathbf{10}^{\mathbf{-0.678}\,\boldsymbol{H}}\boldsymbol{Re_{\delta_2}}^{\mathbf{-0.268}} \tag{12}$$

*Modified Abu-Ghannam and Shaw Model for Transition Prediction[19, 20]*

$$\boldsymbol{\tau'} = \mathbf{2.7}\ \tanh(\boldsymbol{\tau}/\mathbf{2.7}) \tag{13}$$

$$\boldsymbol{\eta_{crit}} = -\mathbf{8.43} - \mathbf{2.4}\ \ln(\boldsymbol{\tau'}/\mathbf{100}) \tag{14}$$

$$\boldsymbol{Re_{\delta_2,tr}} = \mathbf{155} + \mathbf{89.0}\left[\mathbf{0.25}\ \tanh\left(\frac{\mathbf{10}}{\boldsymbol{H}-\mathbf{1}} - \mathbf{5.5}\right) + \mathbf{1}\right]\boldsymbol{\eta_{crit}}^{\mathbf{1.25}} \tag{15}$$

*Mayle's Model for Transition Onset triggered by separation bubbles[21]*

$$\boldsymbol{Re_{s,tr}} - \boldsymbol{Re_{s,sep}} = \mathbf{700}\,\boldsymbol{Re_{\delta_2,sep}}^{\mathbf{0.7}} \tag{16}$$

$$Re_{\Delta s} = 400\, Re_{\delta_2,tr}{}^{0.7} \tag{17}$$

*Stratford's Separation Criterion*[22]

$$\left(x_s - x_f\right)^2 C_p \frac{dC_p}{dx} = 0.0104 \tag{18}$$

*Mayle's Intermittency Model*[21]

$$\gamma(s) = 1 - \exp\left(\eta\sigma \left(Re_s - Re_{s,tr}\right)^2\right) \tag{19}$$

$$\eta\sigma = 2.28\, 10^{-5} / Re_{\delta_2,s}{}^{1.4} \tag{20}$$

As in previous works[12-14], the local $C_f$ value in any position around the airfoil is calculated by a first order model of linear combination of Equations **(3)** and **(12)**:

$$C_f = C_{f,lam} \cdot (1 - \gamma) + C_{f,turb} \cdot \gamma \tag{21}$$

For H, it is used other literature model[19]. One other condition, that is very important to link the laminar to the turbulent flow calculations, it is the momentum thickness assumption where the turbulent boundary-layer starts, $\gamma$ is near zero and transition onset occurrs[12-14]:

$$\delta_{2,lam} = \delta_{2,tr} = \delta_{2,turb} \tag{22}$$

## IV. Numerical Code Implementation

Regarding the code structure, the proposed numerical code works with $C_p$ distribution around airfoil as simple input and does not interact back with the flow by using the displacement thickness of boundary layer. It is not like Xfoil that already has a potential code integrated and does iterative boundary-layer calculations. It is a first approximation – not to have boundary-layer and non-viscous flow iterative solution - that shall be improved in next works by present authors. In sum, the code is able to receive $C_p$ distribution as input from one of two flow solution codes: 1) potential flow of XFoil and; 2) compressible viscous or Euler of CFD++. The compressible RANS viscous flow solution can be laminar, transitional or fully turbulent, or even all together like in Langtry-Menter model.

A first order trapezoidal integration is adopted and implemented in the numerical code to solve the equations for the mathematical model. The grid spacing is fine enough to provide satisfactory accuracy of the results. A sanity check was performed by using high order methods and first order results had acceptable results. The first order integration was also used successfully in previous works[12-14] not only in boundary-layer but coupled with water film subjected to evaporative cooling and also coupled with streamwise thermal conduction. The turbulent boundary-layer equation model, Equations **(6)** to **(12)**, were solved iteratively by using trapezoidal integration instead of Runge-Kutta, which is frequently used in literature[16,17].

Two transition models were implemented: 1) one triggered by natural or by-pass mechanisms, Equations **(13)** to **(15)**; 2) another triggered by laminar separation, Equation **(16)** to **(18)**. Both models work together because they simulate different triggering mechanisms. The one that occurs at most upstream position will define the transition onset. To define the separation position, the present authors selected Stratford criterion because its reliability and accuracy for this kind of studies performed in present paper. Any separation detection criterion using boundary-layer integral parameters like $C_f$, $\lambda$ or $H$ would be affected by the lost of accuracy of the integral method in adverse pressure gradient variation region.

## V. Results and Discussion

The present paper presents three types of analyses in order to understand physical phenomena, to validate proposed numerical code and CFD but also to characterize the aerodynamic performance of the airfoil by CFD in a much broader range than boundary-layer codes are able to do. The first analysis is a local analysis of the boundary-layer by the distribution of the parameters $C_f$ and $H$ around airfoil. This analysis has no direct use for helicopter aerodynamics but has an important use to verify whether the mathematical models are representing the physics. The verification of the local parameters around airfoil is sometimes required because the $C_L$ , $C_D$ and $C_M$ results validation at top level may not guarantee that physics is being modeled adequately. The second analysis performed is the verification of the mean viscous drag coefficient, i.e., $C_{D,viscous} = \overline{C_f}$ . The objective is to show how a local effect like transition occurrence may affect the integrated mean results. The third analysis is the aerodynamic performance for the airfoil at two Re by polar drag and $C_L$ vs. $\alpha$ curves. Those are the results required to perform flight mechanic analysis and the final objective of developing models and validating their results with experimental data. Accurate aerodynamic results will

lead to accurate estimations of helicopter engine power, flight stability and overall mission performance[23], which are key for a successful design as well as market competition.

### A. Local Analysis of $C_f$ and $H$ for Case $C_L$ = 0.57 at Re=$2.6 \cdot 10^6$

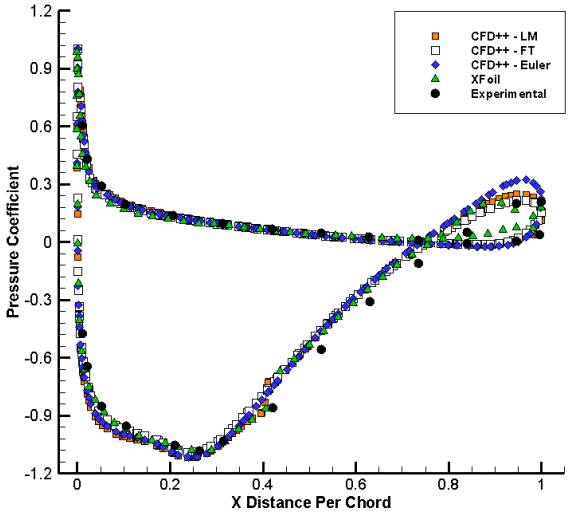


**Figure 1. Distribution of pressure coefficient around the airfoil for Xfoil and CFD++ solutions**

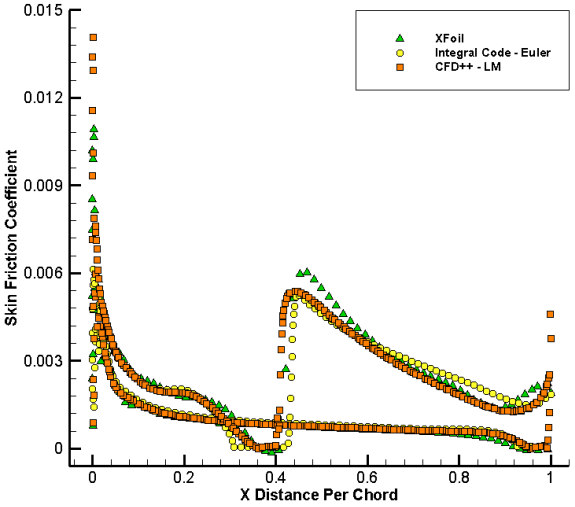


**Figure 2. Skin friction. CFD++ Euler input to integral code compared to CFD++ LM and XFoil.**

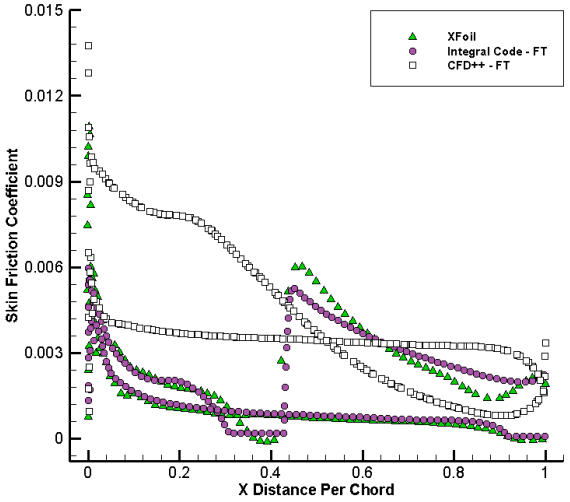


**Figure 3. Skin friction. CFD++ FT input to integral code compared to CFD++ FT and XFoil.**

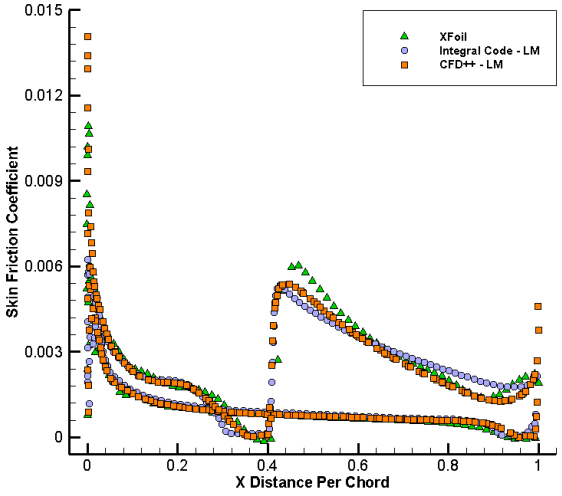


**Figure 4. Skin friction. CFD++ LM input to integral code compared to CFD++ LM and XFoil.**

Figure 1 show the $C_p$ distribution calculated by Xfoil and CFD++ compared to experimental data from NACA report[5] for $C_L$ =0.57 and Re=$2.6 \cdot 10^6$. Both Xfoil and CFD++ found $\alpha$'s necessary to match a $C_L$ =0.57 value as one can see at Table 1. Xfoil and CFD++ LM Model are very close to each other – including in transition region around $X/C$=0.4 - unless the trailing edge where the CFD++ LM is closer to experimental data than Xfoil. As expected the CFD++ fully turbulent and Euler solutions did not capture transition effects. Figure 2 to 4 show $C_f$ distribution around airfoil. The CFD++ fully turbulent overestimates in all range with exception of turbulent region of the upper side. Xfoil has a higher overshoot of $C_f$ downstream the transition region than proposed numerical code and CFD++ LM and a small undershoot upstream the transition onset than CFD++ LM and integral codes. It can be noticed that proposed integral code separates, i.e., $C_f \approx 0$, in a position upstream than other codes. CFD++ and Xfoil have similar results in the adverse pressure gradient variation region just upstream the separation point. As the $C_p$ distributions of CFD++ Euler and Fully Turbulent are very similar along transition point, Figure 1, the $C_f$ distribution result of proposed integral code is also similar, Figures 2 and 3, whether it use Euler or FT results as inputs. Despite Xfoil $C_p$ results can be used as inputs, they are not shown in the present paper.

**Table 1. Angle of Attack found by solvers to match $C_L$ = 0.57 at Re=$2.6 \cdot 10^6$**

| Solver | CFD++ Euler | CFD++ LM | CFD++ FT | XFoil |
|---|---|---|---|---|
| $\alpha$ | 4.39º | 4.39º | 4.17º | 3.62º |

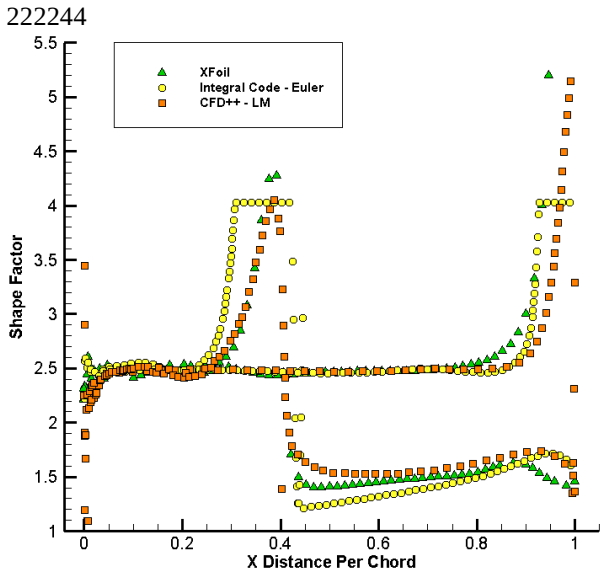


**Figure 5. Shape factor. Euler pressure Coefficient Input to integral code compared to LM Model CFD++ and XFoil.**

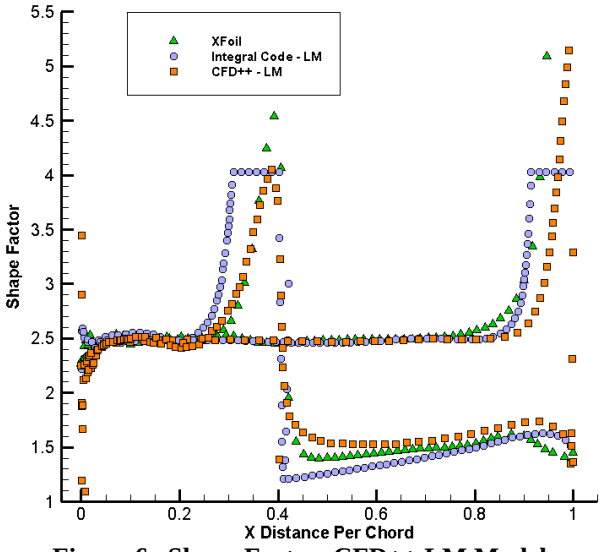


**Figure 6. Shape Factor. CFD++ LM Model pressure coefficient input to integral code compared to LM Model CFD++ and XFoil.**

Figures 2 and 5 present both $C_f$ and $H$ calculations predicted by proposed numerical code when the $C_p$ input used was estimated by CFD++ Euler. On other hand, Figures 3 and 6 show same results but when the input $C_p$ is generated by CFD++ LM. Comparing those four graphics, one can notice that the boundary-layer code will predict separation and transition onset upstream if it uses inviscid Euler solution than LM Turbulence model. In sum, the viscous LM solution is closer to an iterative solution of boundary-layer - as Xfoil does -and flow and non-viscous Euler is a purely non-iterative one-pass solution of the boundary-layer. Finally, Figures 5 and 6 present the $H$ distribution and quantify how much the velocity profile is different between the codes. Those differences are masked or not clear when comparing only $C_f$. It is important to notice that Xfoil has undershoot and overshoots when compared to CFD++ LM, which has a smoother transition than Xfoil and integral code. From integral code results, one can notice that the laminar flow is disturbed in a position more upstream than other codes when approaching separation due to eventual model limitations. However, to know which code is more realistic, comparison with experimental data is required.

### B. Local Analysis of $C_f$ and $H$ for Case $\alpha$ = 3.94º at Re=$2.6 \cdot 10^6$

The value of α = 3.94º is defined by interpolating the $C_L - \alpha$ curve published in NACA report[5] at $C_L$ = 0.57 since the authors did not mention what was the angle of attack of the where the $C_p$ data were measured. Therefore, CFD++ and Xfoil were executed considering this value of angle of attack as input. It is different from previous section because here the $\alpha$ is the same for all flow solvers. Table 1 shows that some solvers required lower angle of attack than others to match same lift. As it may indicate less accuracy for the same angle of attack and both polar drag and lift curves are referred to same angle of attack, it is important to compare all solvers also with same α instead of only same $C_L$.

By inspecting Figure 7, one can conclude that Xfoil provided more lift when executed at same angle of attack of other codes. Its results have more deviation from experimental data and also from CFD++ Euler, FT and LM. CFD++ LM is the solver that has closer results to experimental data than other solutions. At trailing edge region, Xfoil and CFD++ Euler were the codes that provided results with more deviation from experimental data. There is a zoom in transition region in Figure 8 where the CFD++ Full Turbulent and Euler are not affected by transition occurrence but Xfoil and CFD++ LM are. Figure 9 presents skin friction distribution for CFD++ LM compared to the proposed integral code and Xfoil. The simulation at same $\alpha$ when compared to same $C_L$ gives very similar results except that integral code is closer to CFD++ LM results in turbulent region. Regarding $H$ distribution in Figure 10, the simulation at same $\alpha$ made all simulations from CFD++, Xfoil and integral code to be closer together than with same $C_L$. Particularly, the integral code results for $C_f$ and $H$ are very close to those of CFD++ LM.

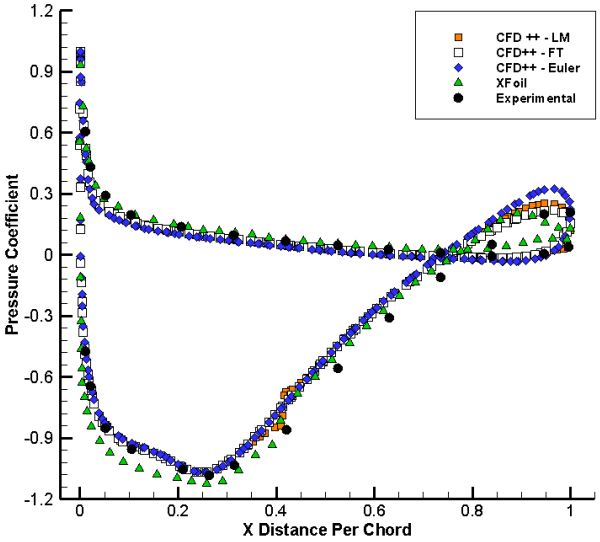


**Figure 7. Distribution of pressure coefficient around the airfoil for Xfoil and CFD++ solutions**

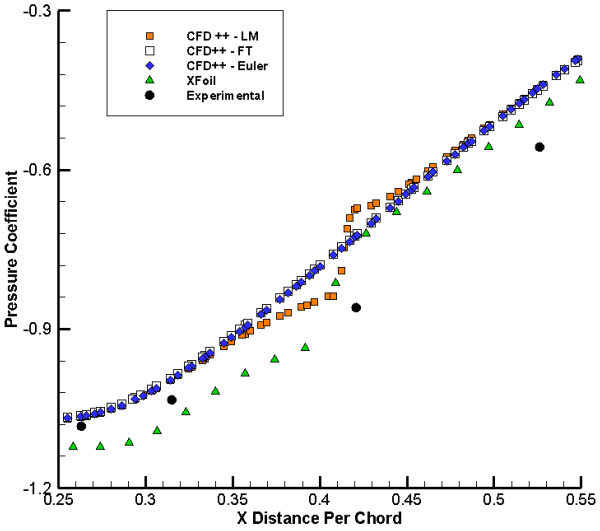


**Figure 8. Zoom at separation and transition region. Distribution of pressure coefficient.**

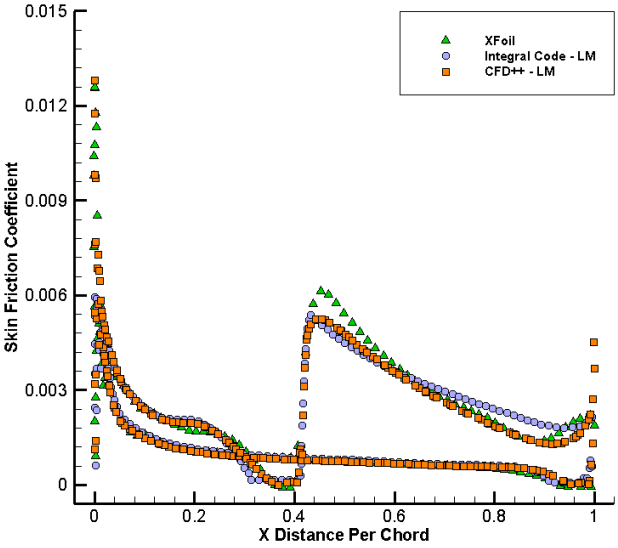


**Figure 9. Skin friction. CFD++ LM input to integral code compared to CFD++ LM and XFoil.**

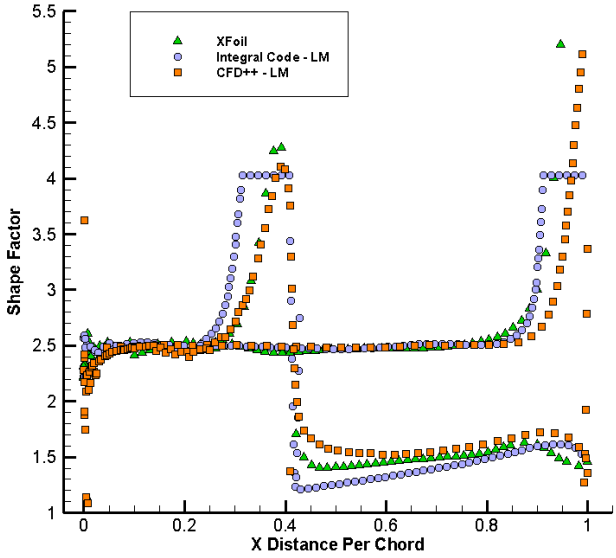


**Figure 10. Shape Factor. CFD++ LM input to integral code compared CFD++ LM and XFoil.**

### C. Mean Skin Friction Comparison

One way to quantify the effect local effects of boundary-layer – like laminar-turbulent transition - on the airfoil drag is to evaluate the differences between calculations of mean skin friction coefficient:

$$C_{D,viscous} = \overline{C_f} = \int_0^1 C_f \frac{dx}{c} \tag{23}$$

Table 2. Integral Viscous Forces Comparison for Re=$\mathbf{2.6 \cdot 10^6}$

| | Same $\alpha$ = 3.94° | | Same CL = 0.57 | |
|---|---|---|---|---|
| | **Integral Code** | **CFD ++** | **Integral Code** | **CFD ++** |
| **Euler** | 0.00341 | ------- | 0.00337 | ------- |
| **Fully Turbulent** | 0.00344 | 0.00779 | 0.00345 | 0.00779 |
| **Transition LM** | 0.00350 | 0.00338 | 0.00348 | 0.00341 |
| **XFoil** | 0.00350 | | 0.00347 | |

The second and fourth columns in Table 1 present the results of the proposed integral code when using the $C_p$ from the CFD++ solutions in the first column – Euler, FT and LM. On the other hand , the third and fifth columns list results of CFD++ viscous solutions calculated with RANS, in this last case no integral code is used. The last line presents the results of Xfoil only since the integral code or CFD++ do not use Xfoil results. In terms of verification of results, integral code with $C_p$ from CFD++ are practiacally the same. The results of CFD++ Fully Turbulent is far from expected values and is almost the double, which demonstrates that for the present cases this type of simulation is not accurate. Despite the transition importance is known for some years in industry projects[24], there is still a lack of validation of CFD local skin friction results around airfoils for transitional flows, mainly due to the few experimental data available in literature[12]. Regarding Table 1, the fact of the CFD++ LM results are lower than integral code and Xfoil does not mean that results are less accurate because there is no experimental data to conclude so. Actually, the next section will demonstrate that CFD++ total drag results – vicous+non-viscous – may sometimes be closer to experimental data[5] than the others.

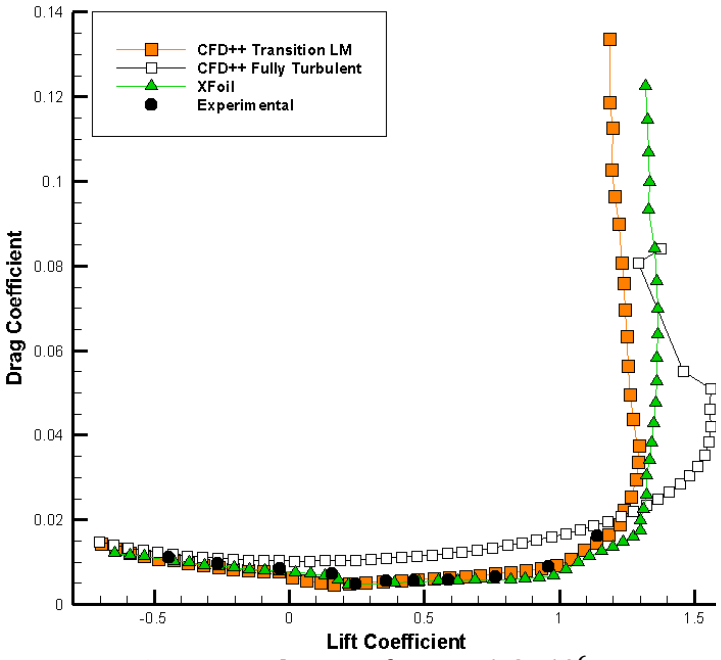


**Figure 11. Polar Drag for Re = $1.8 \cdot 10^6$**

### D. Aerodynamics Performance Results

Figure 11 presents the experimental polar drag curve compared to Xfoil but also CFD++ LM and Fully Turbulent. There is no integral code calculations for the polar drag yet. This validation of integral code is planned to be done in next works by the present authors. It is important to emphasize that the integral code would contribute only with viscous drag but not to non-viscous drag and lift because $C_p$ is calculated by an external solver. In sum, the CFD++ LM results are closer to experimental data than the other solutions. Particularly the Fully Turbulent has deviations in both drag and lift coefficients. In addition, Xfoil results are very close to experimental data when the lift coefficient is lower than unity but starts to have large deviations above that value. This behavior may be due the high angle attack limitations of potential flow code and the boundary layer mathematical model.

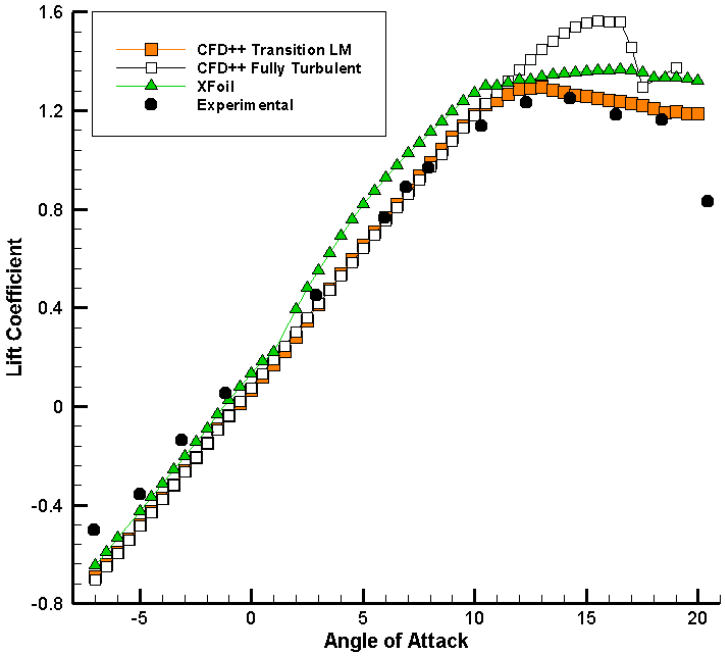


**Figure 12. Angle of attack vs. lift coefficient for Re = $1.8 \cdot 10^6$**

The $C_L - \alpha$ curve of Figure 12 shows that Xfoil results are closer to experimental data than other solutions in range of angle of attack from -5º to 5º and that CFD++ is closer to data in range above 5º. The experimental data may have large measurement errors in range below zero since all solvers predict a linear behavior when data is departing from that. The CFD++ LM capture more accurately the $C_L$

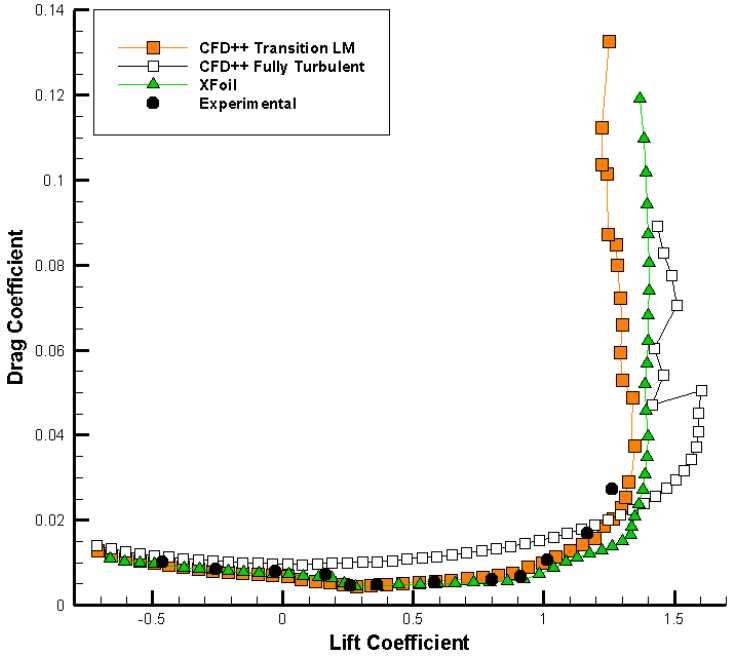


**Figure 13. Polar Drag for Re = $2.6 \cdot 10^6$**

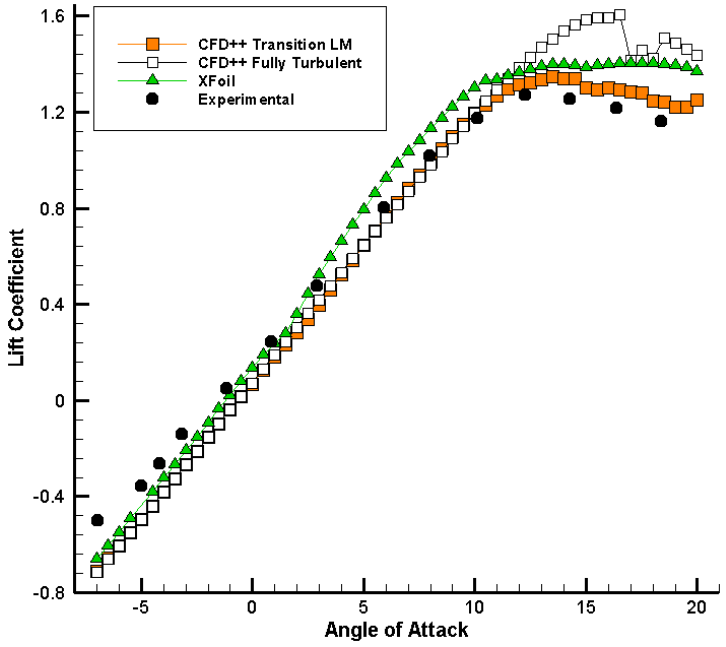


**Figure 14. Angle of attack vs. lift coefficient for Re = $2.6 \cdot 10^6$**

maximum and degradation than other solutions. The largest deviation is noticed at 20º and that may be explained by model difficulties to describe the flow when massive separation occurs. At this high angle may be exist larger measurement errors than low angles due to limitations of the instruments and acquisition to characterize oscillating pressures at that time[5].

To complete the study the present authors also simulated the Re of $2.6 \cdot 10^6$ from the same set of experimental data[5]. Figure 13 shows the polar drag curve with comparisons between the codes and Figure 14 the $C_L - \alpha$ curve with results from all codes also. Also in those cases, CFD++ LM was in general closer to experimental data than other solutions.

In general, the results of fully turbulent solution generate more deviation in polar drag curve than in $C_L - \alpha$ curve, however, it is clear than the $C_L$ maximum prediction and its degradation that are also dependent of an adequate laminar-turbulent transition modeling. Despite the Xfoil has a transition model implemented, it may not captured the $C_L$ maximum as the CFD++ LM did because its limitations to simulate flow accurately high angles of attack, in this case $\alpha > 10°$.

## VI. Conclusion

The results show that laminar-turbulent transition consideration is very important to represent actual airfoil aerodynamics performance. If transition effects are not considered, the helicopter design will be less accurate and could cause deviation in the total power required from engine as well as could affect performance, flight mechanics and its control design estimates. Based on the results obtained in the present paper and on the deviations between numerical results and experimental data, one can make an engineering assessment and use the CFD code to estimate aerodynamic performance of an original or modified NACA 8H12 in other flow conditions, which are outside the validity limits of integral boundary layer tools – like high M and high angles of attack. Despite the CFD++ results were validated against experimental data, they were only performed for integral force coefficients, $C_L$ , $C_D$ and $C_M$, not for local boundary-layer parameters like distributed $C_f, H, \delta_2, \gamma$ around airfoil. This kind of validation with local parameters is certainly required to check accuracy and also improve the laminar-turbulent transition mathematical models implemented in CFD+ but mainly in the proposed integral code.

## VII. References


[1] Drela, M. and Giles, M. B., "Viscous-Inviscid Analysis of Transonic and Low Reynolds Number Airfoils," AIAA Journal, Vol. 25, No. 10, 1986, pp. 1347-1355.

[2] XFoil, Open Source Code, Ver. 6.99, Mark Drela, 2000.

[3] CFD++, Software Package, Ver. 14.1, Metacomp Technologies Inc., 1994

[4]Chakravarthy, S., Peroomian, O., Goldberg, U., and Palaniswamy, S., 1998. "The CFD++ computational fluid dynamics software suite". In Proc. World Aviation Congress and Exposition, 1998, Anaheim, Society of Automotive Engineers, 1998, SAE Paper 985564

[5] Stivers, L. S. and Rice, F. J., "Aerodynamic Characteristics of Four NACA Airfoil Sections Designed for Helicopter Rotor Blades", NACA Report Nº L5K02, February, 1946.

[6] Goldberg, U., Peroomian, O., and Chakravarthy S. "A Wall-Distance-Free k-e Model With Enhanced Near-wall Treatment," ASME J. Fluids Engrg., volume 120, pages 457-462, September 1998

[7] Langtry, R. B., Menter, F. R., Likki, S. R., Suzen, Y. B., Huang, P. G. and Volker, S., "A Correlation-Based Transition Model Using Local Variables - Part II: Test Cases and Industial Aplications", Journal of Turbomachinery, Vol. 128, July 2006, pp. 423-434.

[8] Langtry, R. B., Menter, F. R., Likki, S. R., Suzen, Y. B., Huang, P. G. and Volker, S., "A Correlation-Based Transition Model Using Local Variables - Part I: Model Formulation", Journal of Turbomachinery, Vol. 128, July 2006, pp. 413-422.

[9] Langtry, R. B., Menter, F. R., Likki, S. R., Suzen, Y. B., Huang, P. G. and Volker, S., "A Correlation-Based Transition Model Using Local Variables - Part II: Test Cases and Industial Aplications", Journal of Turbomachinery, Vol. 128, July 2006, pp. 423-434.

[10]Tobaldini Neto, L., Pimenta, M.M., Silva, G.A.L., "Laminar-Turbulent Transition Modeling Strategies for Thermally Protected Airfoils", In Paper no. FEDSM2008-55284, ASME, American Socitey of Mechanical Engineers, pp. 9, 2008, ASME 2008 Fluids Engineering Division Summer Meeting (FEDSM2008) , Jacksonville, 2008.

[11] Kays, W. M., and Crawford, M. E., Convective Heat and Mass Transfer, 3rd ed., McGraw-Hill, New York, 1993.

[12] Silva, G. A. L., "Transferência de Calor e Massa no Escoamento Bifásico em Torno de Aerofólios Equipados com Sistemas de Antigelo Aeronáuticos," Ph.D. Dissertation, Escola Politécnica da Universidade de São Paulo Dept., Mechanical Engineering., São Paulo, SP, 2009.

[13]Silva, G. A. L. and Silvares O. M. and Zerbini, E. J. G. J, Numerical Simulation of Airfoil Thermal Anti-ice Operation. Part 1: Mathematical Modeling, Journal of Aircraft, 44, 2, 2007, Mach-April.

[14]Silva, G.A.L., Silvares, O.M., Zerbini, E.J.G.J., Hefazi, H., Chen, H.H. and Kaups, K. , Differential Boundary-Layer Analysis and Runback Water Flow Model Applied to Flow Around Airfoils with Thermal Anti-ice , AIAA Aerospace Sciences and Meeting, Reston, American Insitute of Aeronautics and Astronautics, pp. 1-12, 2009.

[15] Walz, A., Boundary Layers of Flow and Temperature, The M.I.T. Press, Massachusetts, 1969.

[16] Cebeci, T., and Bradshaw, P., Physical and Computational Aspects of Convective Heat Transfer, 2nd ed., Horizons Publishing, Long Beach, 2005.

[17] Cebeci, T., and Cousteix, J., Modeling and Computation of Boundary-Layer Flows, Springer-Verlag, New York, 1984.

[18] Head, M. R., "Entrainment in the Turbulent Boundary Layers" ARC R&M 3152, 1958.

[19]Abu-Ghannam, B. J. and Shaw, R., "Natural Transition of Boundary Layers - The Effects of Turbulence Pressure Gradient, and Flow History," Journal Mechanical Engineering Science, Vol. 22, No. 5, 1980, pp. 213-228.

[20] Drela, M.,"MISES Implementation of Modified Bu-Ghannam/Shaw Transition Criterion," MIT Aero-Astro [online database], July 198, URL: http://web.mit.edu/drela/Public/web/mises/ [cited 14 December 2009].

[21] Mayle, R. E. (ed.), "The Role of Laminar-Turbulent Transition in Gas Turbine Engines," Journal of Turbomachinery, Vol. 113, 1991, pp. 509-537.

[22] Stratford, B. S., "Flow in the Laminar Boundary Layer near Separation" Repors and Memoranda Nº 3002, November 1954.

[23] Leishman, J. G., Principles of Helicopter Aerodynamics, 2nd ed., Cambridge, New York, 2006.

[24] Spalart, P.R., "Topics in industrial viscous flow calculations" In: Henkes, R.A.W.M., Van Ingen, J.L. Transitional Boundary Layers in Aeronautics. Amsterdam, North-Holland, Ch. 5, p 269-82